Onset of quantum chaos in one-dimensional bosonic and fermionic systems and its relation to thermalization

Lea F. Santos*
Department of Physics, Yeshiva University, New York, New York 10016, USA

Marcos Rigol†
Department of Physics, Georgetown University, Washington, D.C. 20057, USA

(Received 12 October 2009; published 5 March 2010)

By means of full exact diagonalization, we study level statistics and the structure of the eigenvectors of one-dimensional gapless bosonic and fermionic systems across the transition from integrability to quantum chaos. These systems are integrable in the presence of only nearest-neighbor terms, whereas the addition of next-nearest-neighbor hopping and interaction may lead to the onset of chaos. We show that the strength of the next-nearest-neighbor terms required to observe clear signatures of nonintegrability is inversely proportional to the system size. Interestingly, the transition to chaos is also seen to depend on particle statistics, with bosons responding first to the integrability breaking terms. In addition, we discuss the use of delocalization measures as main indicators for the crossover from integrability to chaos and the consequent viability of quantum thermalization in isolated systems.

DOI: 10.1103/PhysRevE.81.036206 PACS number(s): 05.45.Mt, 05.30.−d, 05.70.Ln, 02.30.Ik

I. INTRODUCTION

Random matrix theory (RMT) deals with the statistical properties of ensembles of matrices composed of random elements. It was originally designed by Wigner in his efforts to understand the statistics of energy levels of nuclei [1] and was further elaborated by several authors, notably Mehta [2]. RMT received a significant boost with the discovery of its connection with classical chaos [3–6]. In particular, it was observed that quantum systems whose classical analog are chaotic show the same fluctuation properties predicted by RMT.

The application of RMT was soon extended to the description of other quantum many-body systems, such as atoms, molecules, and quantum dots [7–10], and it was not restricted to statistics of eigenvalues but accommodated also the analysis of eigenstates [11–13]. Important developments that led to the broadening of the theory include the introduction of ensembles of random matrices that take into account the predominance of short-range interactions in real many-body systems [14–16], the intimate connection between quantum transport and spectral properties of mesoscopic systems [8,17,18], and the relationship between chaos and quantum thermalization [12,19–24].

It has been conjectured that the thermalization of finite isolated quantum systems is closely related to the onset of chaos and occurs at the level of individual states [19,20,25], which has become known as the eigenstate thermalization hypothesis (ETH). Related work was done with nuclear shell model calculations and delocalization measures [26,12]. More recently, this subject has received renewed attention due to its relevance to ultracold gas experiments. For example, in a remarkable experiment by a group at Penn State [27], it was shown that, after being subject to a strong perturbation, a gas of bosons trapped in a (quasi-)one-dimensional geometry (created by means of a deep two-dimensional optical lattice) did not relax to the standard prediction of statistical mechanics. In contrast to those results, in another experiment in which a bosonic gas was trapped in a different (quasi-)one-dimensional geometry (generated by an atom chip), relaxation to a thermal state was inferred to occur in a very short time scale [28].

Following those experiments, several theoretical works have explored the question of thermalization in nonintegrable isolated quantum systems after a quantum quench in one dimension [29–37]. After numerically exploring the nonequilibrium dynamics in finite one-dimensional (1D) systems, thermalization was observed in some regimes [29–32] but not in others [29–32], even though in all cases integrability was broken. Several factors may play a role in the absence of thermalization in finite 1D systems after a quench: (i) the proximity to integrable points [31,32], (ii) the proximity of the energy of the initial nonequilibrium state after the quench to the energy of the ground state [31,32,37], (iii) particle statistics and the observable considered (in fermionic systems, the momentum distribution function may take much longer to relax to equilibrium than other observables [32]), and finally (iv) quenching the system across a superfluid/metal to insulator transition [29,30,37]. Recent numerical studies for bosons and fermions in one dimension have shown that there is a direct link between the presence (absence) of thermalization and the validity (failure) of the ETH [31,32].

In the present work, we provide a detailed description of the integrable-chaos transition in the one-dimensional bosonic and fermionic systems studied in Refs. [31,32]. These systems are clean and have only two-body interactions; the transition to chaos is achieved by increasing the strength of next-nearest-neighbor (NNN) terms rather than by adding random parameters to the Hamiltonian. Under cer-

*lsantos2@yu.edu
†mrigol@physics.georgetown.edu

tain conditions these systems may also be mapped onto Heisenberg spin-1/2 chains. Several papers have analyzed spectral statistics of disordered [38–42] and clean [43–46] 1D Heisenberg spin-1/2 systems. Mostly, they were limited to sizes smaller than considered here and, in the case of clean systems, focused on properties associated with the energy levels, while here eigenvectors are also analyzed. Our goal is to establish a direct comparison between indicators of chaoticity and the results obtained in Refs. [31,32] for thermalization and the validity of ETH. Our analysis also provides a way to quantify points (i) and (ii) in the previous paragraph, which can result in the absence of thermalization in finite systems.

Overall, the crossover from integrability to chaos, quantified with spectral observables and delocalization measures, mirrors various features of the onset of thermalization investigated in Refs. [31,32], in particular, the distinct behavior of observables between systems that are close and far from integrability, and between eigenstates whose energies are close and far from the energy of the ground state. We also find that the contrast between bosons and fermions pointed out in Ref. [32] is translated here into the requirement of larger integrability breaking terms for the onset of chaos in fermionic systems. Larger system sizes also facilitate the induction of chaos. In addition, we observe that measures of the degree of delocalization of eigenstates become smooth functions of energy only in the chaotic regime, a behavior that may be used as a signature of chaos.

The paper is organized as follows. Section II describes the model Hamiltonians studied and their symmetries. Section III analyzes the integrable-chaos transition based on various quantities. After a brief review of the unfolding procedure, Sec. III A focuses on quantities associated with the energy levels, such as level spacing distribution and level number variance. Section III B introduces measures of state delocalization, namely, information entropy and inverse participation ratio (IPR), showing results for the former in the mean-field basis. Results for the inverse participation ratio and discussions about representations are left to the Appendix. Concluding remarks are presented in Sec. IV.

II. SYSTEM MODEL

We consider both scenarios: hard-core bosons and spinless fermions on a periodic one-dimensional lattice in the presence of nearest-neighbor (NN) and NNN hopping and interaction. The Hamiltonian for bosons H_B and for fermions H_F are, respectively, given by

$$H_B = \sum_{i=1}^{L} \left[-t(b_i^\dagger b_{i+1} + \text{H.c.}) + V\left(n_i^b - \frac{1}{2}\right)\left(n_{i+1}^b - \frac{1}{2}\right) - t'(b_i^\dagger b_{i+2} + \text{H.c.}) + V'\left(n_i^b - \frac{1}{2}\right)\left(n_{i+2}^b - \frac{1}{2}\right)\right], \quad (1)$$

$$H_F = \sum_{i=1}^{L} \left[-t(f_i^\dagger f_{i+1} + \text{H.c.}) + V\left(n_i^f - \frac{1}{2}\right)\left(n_{i+1}^f - \frac{1}{2}\right) - t'(f_i^\dagger f_{i+2} + \text{H.c.}) + V'\left(n_i^f - \frac{1}{2}\right)\left(n_{i+2}^f - \frac{1}{2}\right)\right]. \quad (2)$$

TABLE I. Dimensions of subspaces.

Bosons				
$L=18$	$k=1,5,7$	$k=2,4,8$	$k=3$	$k=6$
	1026	1035	1028	1038
$L=21$	$k=7$	other k's		
	5538	5537		
$L=24$	odd k's	$k=2,6,10$	$k=4$	$k=8$
	30624	30664	30666	30667
Fermions				
$L=18$	$k=1,5,7$	$k=2,4,8$	$k=3$	$k=6$
	1035	1026	1038	1028
$L=21$	$k=7$	other k's		
	5538	5537		
$L=24$	odd k's	$k=2,6,10$	$k=4$	$k=8$
	30624	30664	30667	30666

Above, L is the size of the chain, b_i and $b_i^\dagger$ (f_i and $f_i^\dagger$) are bosonic (fermionic) annihilation and creation operators on site i, and $n_i^b = b_i^\dagger b_i$ ($n_i^f = f_i^\dagger f_i$) is the boson (fermion) local density operator. Hard-core bosons do not occupy the same site, i.e., $b_i^{\dagger 2} = b_i^2$, so the operators commute on different sites but can be taken to anticommute on the same site. The NN (NNN) hopping and interaction strengths are, respectively, t (t') and V (V'). Here, we only study repulsive interactions ($V, V' > 0$). We take $\hbar = 1$ and $t = V = 1$ set the energy scale in the remaining of the paper.

The bosonic (fermionic) Hamiltonian conserves the total number of particles N_b (N_f) and is translational invariant, being therefore composed of independent blocks each associated with a total momentum k. In the particular case of $k=0$, parity is also conserved and, at half-filling, particle-hole symmetry is present, that is, the bosonic [fermionic] model becomes invariant under the transformation $\Pi_i^L(b_i^\dagger + b_i)$ [$\Pi_i^L(f_i^\dagger + f_i)$], which annihilates particles from filled sites and creates them in empty ones. The latter two symmetries will be avoided here by selecting $k \neq 0$ and $N_{b,f} = L/3$. For even L, we consider $k = 1, 2, \ldots, L/2-1$ and, for odd L, $k = 1, 2, \ldots, (L-1)/2$. The dimension D_k of each symmetry sector studied is given in Table I.

Exact diagonalization is performed to obtain all eigenvalues and eigenvectors of the systems under investigation. When $t' = V' = 0$, models (1) and (2) are integrable and may be mapped onto one another via the Jordan-Wigner transformation [47]. A correspondence with the Heisenberg spin-1/2 chain also holds, in which case the system may be solved with the Bethe ansatz [48,49].

III. SIGNATURES OF QUANTUM CHAOS

The concept of exponential divergence, which is at the heart of classical chaos, has no meaning in the quantum domain. Nevertheless, the correspondence principle requires that signatures of classical chaos remain in the quantum

level. Different quantities exist to identify the crossover from the integrable to the nonintegrable regime in quantum systems. We consider both spectral observables associated with the eigenvalues and quantities used to measure the complexity of the eigenvectors.

A. Spectral observables

Spectral observables, such as level spacing distribution and level number variance are investigated below. They are intrinsic indicators of the integrable-chaos transition. Their analyses are based on the unfolded spectrum of each symmetry sector separately.

1. Unfolding procedure

The procedure of unfolding consists of locally rescaling the energies as follows. The number of levels with energy less than or equal to a certain value E is given by the cumulative spectral function, also known as the staircase function, $N(E)=\Sigma_n\Theta(E-E_n)$, where Θ is the unit step function. $N(E)$ has a smooth part $N_{sm}(E)$, which is the cumulative mean level density, and a fluctuating part $N_{fl}(E)$, that is, $N(E)=N_{sm}(E)+N_{fl}(E)$. Unfolding the spectrum corresponds to mapping the energies $\{E_1,E_2,\ldots,E_D\}$ onto $\{\epsilon_1,\epsilon_2,\ldots\epsilon_D\}$, where $\epsilon_n=N_{sm}(E_n)$, so that the mean level density of the new sequence of energies is 1. Different methods are used to separate the smooth part from the fluctuating one. Statistics that measure long-range correlations are usually very sensitive to the adopted unfolding procedure, while short-range correlations are less vulnerable [50]. Here, we discard 20% of the energies located at the edges of the spectrum, where the fluctuations are large, and obtain $N_{sm}(E)$ by fitting the staircase function with a polynomial of degree 15.

2. Level spacing distribution

The distribution of spacings s of neighboring energy levels [2,7,8,10] is the most frequently used observable to study short-range fluctuations in the spectrum. Quantum levels of integrable systems are not prohibited from crossing and the distribution is Poissonian, $P_P(s)=\exp(-s)$. In nonintegrable systems, crossings are avoided and the level spacing distribution is given by the Wigner-Dyson distribution, as predicted by random matrix theory. The form of the Wigner-Dyson distribution depends on the symmetry properties of the Hamiltonian. Ensembles of random matrices with time-reversal invariance, the so-called Gaussian orthogonal ensembles (GOEs), lead to $P_{WD}(s)=(\pi s/2)\exp(-\pi s^2/4)$. The same distribution form is achieved for models (1) and (2) in the chaotic limit since they are also time-reversal invariant. However, these systems differ from GOEs in the sense that they only have two-body interactions and do not contain random elements. Contrary to GOEs and to two-body random ensembles [15], the breaking of symmetries here is not caused by randomness, but instead by the addition of frustrating next-nearest-neighbor couplings. Notice also that the analysis of level statistics in these systems is meaningful only in a particular symmetry sector; if different subspaces are mixed, level repulsion may be missed even if the system is chaotic [46,51].

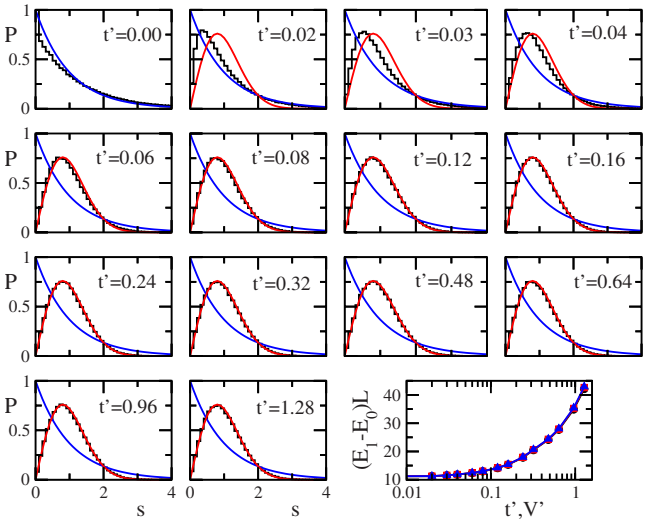

FIG. 1. (Color online) Level spacing distribution for hard-core bosons averaged over all k's in Table I, for $L=24$, and $t'=V'$. For comparison purposes, we also present the Poisson and Wigner-Dyson distributions. Bottom right panel: energy difference between first excited state E_1 and ground state E_0 in the full spectrum times L, for $L=18$ (circles), 21 (squares), and 24 (triangles).

In Figs. 1 and 2, we show $P(s)$ across the transition from integrability to chaos for bosons and fermions, respectively, in the case of $L=24$. An average over all k's is performed, but we emphasize that the same behavior is verified also for each k sector separately. As t',V' increases and symmetries are broken, level repulsion becomes evident, the peak position of the distribution shifts to the right, and the tail of the distribution changes from exponential to Gaussian. Excellent agreement with the Wigner-Dyson distribution is seen already for $t'=V'>0.12$. The bottom right panels in Figs. 1 and 2 give the energy difference between first excited state and ground state times L as a function of t',V'. One can see there that the product is size independent emphasizing that the ground state of the systems considered here is gapless in the thermodynamic limit, as expected from the phase dia-

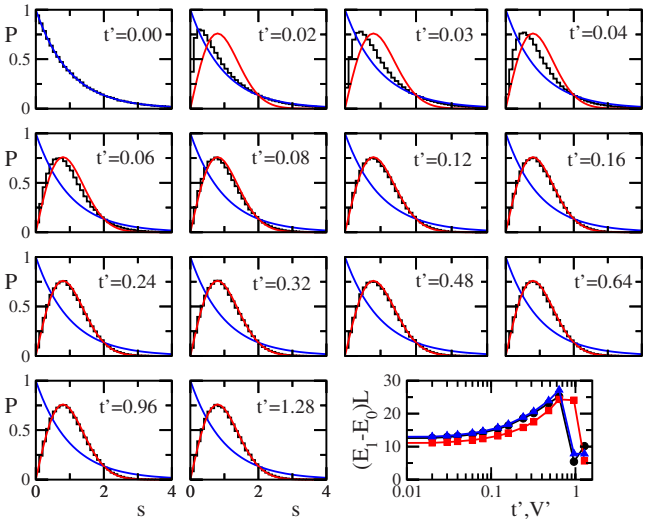

FIG. 2. (Color online) As in Fig. 1 but for spinless fermions.

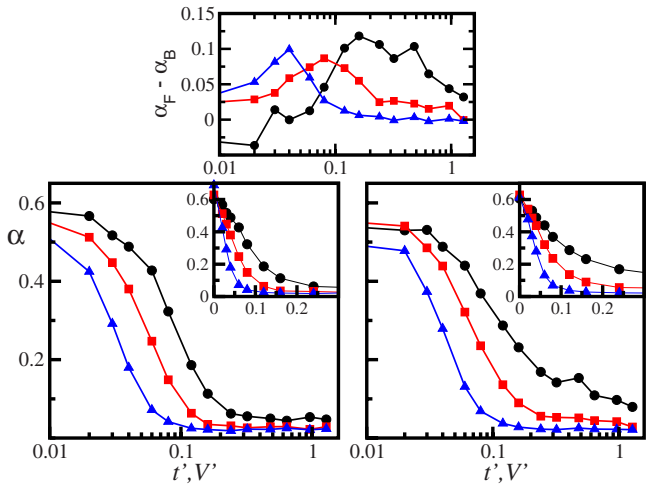

FIG. 3. (Color online) Average α over all k's; $t'=V'$. Top panel: difference α(fermions)$-\alpha$(bosons). Left bottom panel, bosons; right bottom panel, fermions. Semilogarithmic plot in main panels and linear plot in insets. Circles, $L=18$; squares, $L=21$; triangles, $L=24$.

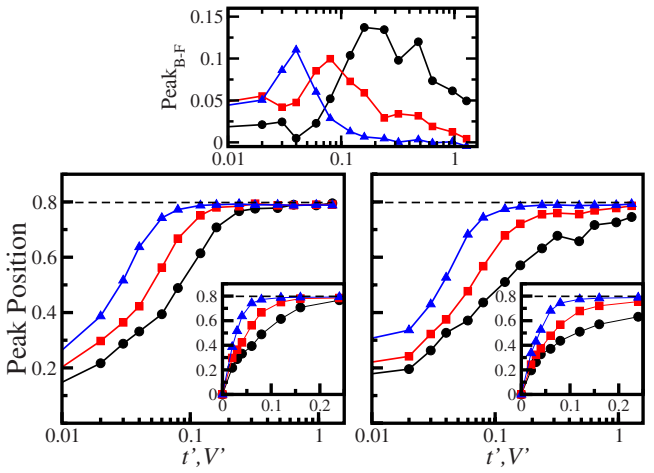

FIG. 4. (Color online) Peak position of the level spacing distribution averaged over all k's; $t'=V'$. Top panel, difference between the peak position of bosons and fermions, peak(bosons) $-$peak(fermions). Left bottom panel, bosons; right bottom panel, fermions. Semilogarithmic plot in main panels and linear plot in insets. Circles, $L=18$; squares, $L=21$; triangles, $L=24$. Dashed line indicates the peak position of $P_{WD}(s)$.

grams presented in Ref. [52]. Notice that the particular case of the fermions exhibits an even-odd finite-size effect that becomes irrelevant in the thermodynamic limit.

To better quantify the integrable-chaos transition, we show in Fig. 3 the level spacing indicator α, defined as follows:

$$\alpha \equiv \frac{\sum_i |P(s_i) - P_{WD}(s_i)|}{\sum_i P_{WD}(s_i)}, \tag{3}$$

where the sums runs over the whole spectrum. We should stress that this is a discrete rather than integral sum, because $P(s)$ as computed by us is a discrete quantity. For a chaotic system $\alpha \to 0$. The indicator α is comparable to the quantity η introduced in Ref. [22].

As seen from the bottom panels and insets in Fig. 3, the values of t', V' leading to the transition to chaos decrease with the size of the system, suggesting that the onset of chaos in the thermodynamic limit might be achieved with an infinitesimally small integrability breaking term, although the existence of a saturation value cannot be discarded [45]. A conclusive statement would require even larger systems or a theory for the behavior of systems approaching infinite sizes. Interestingly, α decays faster for bosons, which indicates that the crossover to the chaotic behavior may depend on particle statistics. This contrasts studies of the ground-state properties of many-body systems with two-body interactions, where such differences were not found [53]. The top panel in Fig. 3 shows the difference between the value of α for fermions and bosons. In general, it diminishes with increasing the size of the chain, and the point at which the difference attains its maximum value moves toward lower values of t', V'.

The findings in Fig. 3 are reinforced in Fig. 4, where we show the approach of the peak position of the level spacing distribution to the peak position of $P_{WD}(s)$ as t', V' increases. The transition is faster for larger chains and once again depends on particle statistics, with bosons responding first to the breaking of symmetries. We should add that equivalent results are obtained by fitting $P(s)$ with the Brody distribution [15],

$$P_B(s) = (\beta+1)bs^{\beta} \exp(-bs^{\beta+1}), \quad b = \left[\Gamma\left(\frac{\beta+2}{\beta+1}\right)\right]^{\beta+1},$$

and analyzing how the increase in t', V' changes β from 0 (in the integrable region) to 1 (in the chaotic limit).

The spectral properties of models (1) and (2) discussed here are somehow mirrored by their dynamical behavior, which were studied, respectively, in Refs. [31,32]. (Notice that the analysis of the integrable-chaos transition performed here uses the same values of t', V' considered in those works.) The smooth approach to integrability, as shown in the figures 1–4 above, is followed by the breakdown of thermalization observed in Refs. [31,32]. However, an important difference between our results here and the results in Refs. [31,32] is that in the latter works it was not clear that the values of t', V' required for the system to thermalize would reduce with increasing system size, whereas this is the case here for obtaining a Wigner-Dyson distribution of the level spacings.

Another interesting feature found in Ref. [32] is that in the context of quenched dynamics there are differences associated with the particle statistics. In particular, it was seen that some observables such as the momentum distribution function $[n(k)]$ in fermionic systems may take longer to relax to equilibrium than their bosonic counterparts. (A related effect in which a quasisteady regime occurs for $n(k)$ before full relaxation has been suggested for higher-dimensional fermionic systems [54–56].) It was also shown in Ref. [32] that

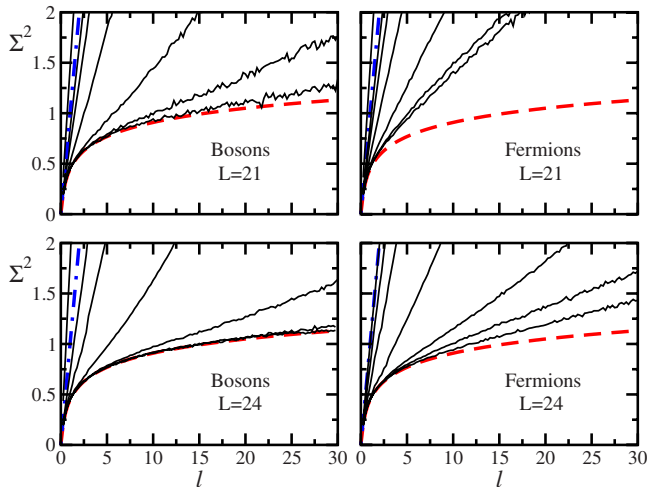

FIG. 5. (Color online) Level number variance averaged over all k's. In each panel, solid lines from top to bottom, $t'=V'=0,0.02,0.04,0.08,0.16,0.32,0.64$. Dashed line, GOE; dotted-dashed line, Poisson.

the difference between the eigenstate expectation values of $n(k)$ for eigenstates of the fermionic Hamiltonian with close energies suffer from particularly large finite-size effects when compared to other observables such as the density-density structure factor $[N(k)]$ and when compared to $n(k)$ and $N(k)$ for hard-core bosons. Interestingly, here we find that for these finite-size systems the measures of chaoticity also exhibit differences between hard-core bosons and fermions, where the former ones respond first to the integrability breaking terms. Further studies will be required to explore the relation between the latter finding and the onset of ETH for different observables and different particle statistics in 1D systems.

3. Level number variance

Other quantities sensitive to spectral fluctuations include measures of long-range correlations, such as spectral rigidity and level number variance [8]. Both are closely related and measure the deviation of the staircase function from the best-fit straight line. Here, we show results for the level number variance $\Sigma^2(l)$ defined as

$$\Sigma^2(l) \equiv \langle [N(l,\epsilon)]^2 \rangle - \langle N(l,\epsilon) \rangle^2, \tag{4}$$

where $N(l,\epsilon)$ gives the number of states in the interval $[\epsilon,\epsilon+l]$ and $\langle\cdot\rangle$ represents the average over different initial values of ϵ. For a Poisson distribution, $\Sigma^2(l)=l$, while for GOEs in the limit of large l, $\Sigma^2(l)=2[\ln(2\pi l)+\gamma+1-\pi^2/8]/\pi^2$, where γ is the Euler constant. Level repulsion leads to rather rigid spectra and fluctuations become much less significant than in the random energy sequences of regular systems.

As expected, the level number variance shown in Fig. 5 approaches the GOE curve as the strength of NNN interactions increases. The proximity to the GOE result also improves as the system size increases. However, deviations from the GOE curve are verified for values of t',V' where the level spacing distribution is already very close to a Wigner-Dyson, especially in the case of fermions (right panels). In fact, the distinct behavior associated with particle statistics becomes yet more evident when studying $\Sigma^2(l)$. The level number variance for the bosonic system with $L=24$, for example, coincides with the GOE result for a large range of values of l already when $t',V'=0.32$ and 0.64, whereas the same is not verified for fermions. This further supports the view that particle statistics may play an important role in the relaxation dynamics and thermalization of finite isolated quantum systems. On the other hand, the size dependence of the results is an indicator that in the thermodynamic limit the differences between the quantities discussed in this paper may become negligible when comparing bosons and fermions, a conjecture that deserves further investigation together with its implications for the dynamics and thermalization of those systems.

B. Delocalization measures

Contrary to spectral observables, quantities used to measure the complexity of eigenvectors, as delocalization measures [11,12], are not intrinsic indicators of the integrable-chaos transition since they depend on the basis in which the computations are performed. The choice of basis is usually physically motivated. The mean-field basis is the most appropriate representation to separate global from local properties, and therefore capture the transition from regular to chaotic behavior [12]. Here, this basis corresponds to the eigenstates of the integrable Hamiltonian $(t',V'=0)$. Other representations may also provide relevant information, such as the site basis, which is meaningful in studies of spatial localization, and the momentum basis, which can be used to study k-space localization (see the Appendix for further discussions).

The degree of complexity of individual eigenvectors may be measured, for example, with the information (Shannon) entropy S or the IPR. The latter is also sometimes referred to as number of principal components. For an eigenstate ψ_j written in the basis vectors ϕ_k as $\psi_j=\Sigma_{k=1}^{D} c_j^k \phi_k$, S and IPR are, respectively, given by

$$S_j \equiv -\sum_{k=1}^{D} |c_j^k|^2 \ln |c_j^k|^2, \tag{5}$$

$$\mathrm{IPR}_j \equiv \frac{1}{\sum_{k=1}^{D} |c_j^k|^4}. \tag{6}$$

The above quantities measure the number of basis vectors that contribute to each eigenstate, that is, how much delocalized each state is in the chosen basis.

For the GOE, the amplitudes c_j^k are independent random variables and all eigenstates are completely delocalized. Complete delocalization does not imply, however, that $S=\ln D$. For a GOE, the weights $|c_j^k|^2$ fluctuate around $1/D$ and the average over the ensemble is $S_{\mathrm{GOE}}=\ln(0.48D)+\mathcal{O}(1/D)$ [11,12].

Figures 6 and 7 show the Shannon entropy in the mean-field basis S_{mf} vs the effective temperature for bosons and

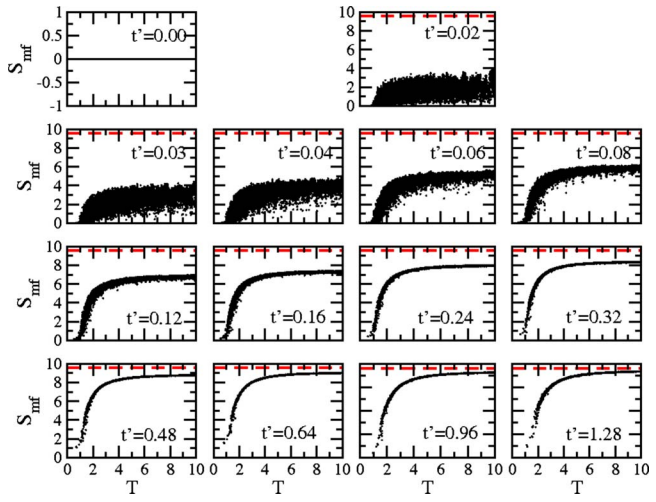

FIG. 6. (Color online) Shannon entropy in the mean-field basis vs effective temperature for bosons, $L=24$, $k=2$, and $t'=V'$. The dashed line gives the GOE averaged value $S_{\mathrm{GOE}}\sim\ln(0.48D)$.

fermions, respectively. The effective temperature T_j of an eigenstate ψ_j with energy E_j is defined as

$$E_j = \frac{1}{Z}\mathrm{Tr}\{\hat{H}e^{-\hat{H}/T_j}\}, \tag{7}$$

where

$$Z = \mathrm{Tr}\{e^{-\hat{H}/T_j}\}. \tag{8}$$

Above, $\hat{H}$ is Hamiltonian (1) or (2), Z is the partition function with the Boltzmann constant $k_B=1$, and the trace is performed over the full spectrum as in Refs. [31,32] (see the Appendix for a comparison with effective temperatures obtained by tracing over exclusively the sector $k=2$). The figures include results only for $T_j\leq 10$; for high E_j, the temperatures eventually become negative. By plotting the Shannon entropy as a function of the effective temperature, we allow for a direct comparison of our results here and the results presented in Refs. [31,32].

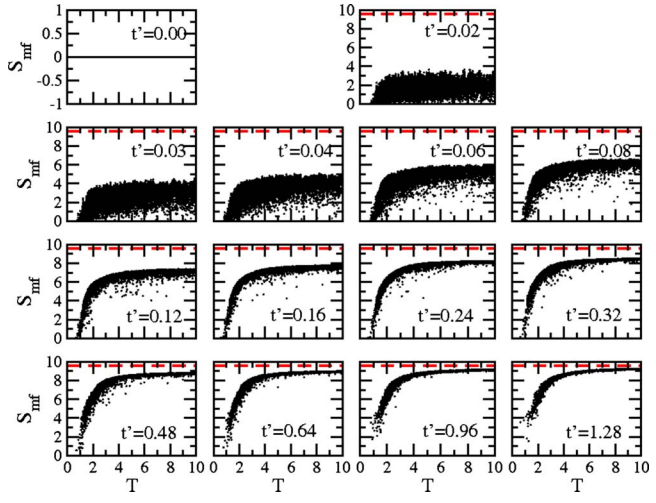

FIG. 7. (Color online) As in Fig. 6 for fermions.

As seen in Figs. 6 and 7, the mixing of basis vectors, and therefore the complexity of the states, increases with t',V', but it is only for $T_j\gtrsim 2$ that the eigenstates of our systems approach the GOE result. Similarly, in plots of S_{mf} vs energy (see Figs. 11 and 12 in the Appendix), it is only away from the borders of the spectrum that $S_{mf}\rightarrow S_{\mathrm{GOE}}$; in the borders, the states are more localized and therefore less ergodic. This feature is typical of systems with a finite range of interactions, such as models (1) and (2) and also banded, embedded random matrices, and two-body random ensembles [13,15,57].

The analysis of the structure of the eigenstates hints on what to expect for the dynamics of the system. In the context of relaxation dynamics, not only the density of complex states participating in the dynamics is relevant, but also how similar these states are. In close connection, but from a static perspective, it is the onset of chaos that guarantees the uniformization of the eigenstates. According to Percival's conjecture [58], the complexity of chaotic wave functions adjacent in energy is very similar; they essentially show the same information entropy. A further extension of this idea is Berry's conjecture [59], which assumes that energy eigenfunctions in a time-reversal invariant and ergodic system are a superposition of random plane waves. The ETH [20] can be related to the validity of Berry's conjecture. ETH states that thermalization of an isolated quantum system occurs when each eigenstate already exhibits a thermal value for the observables, that is, the eigenstate expectation values do not fluctuate between eigenstates close in energy.

In Figs. 6 and 7 (see also Figs. 11–16 in the Appendix), the structure of the eigenstates close in energy reveals fluctuations throughout the spectrum as we approach integrability, whereas in the chaotic regime, fluctuations are mostly restricted to the edges of the spectrum, with S_{mf} being a smooth function of energy (or temperature) away from the borders. A related result was seen in Ref. [41], where a clear relationship between an entanglement measure and a delocalization measure for a clean Heisenberg model appeared only in the chaotic limit (two dimensions), being absent in its integrable counterpart (one dimension). Fluctuations imply that eigenstates very close in energy have different degrees of complexity and localization properties; these states may therefore not entirely comply with the ETH. This explains the absence of thermalization in the integrable limit. In fact, a similar conclusion was achieved in Refs. [31,32] based on plots for the momentum distribution function vs energy (Figs. 4 and 7, respectively). There, it was observed that fluctuations between expectation values of states close in energy increase toward integrability.

Two additional points need to be made here. First, even in the chaotic regime one sees that states in the edge of the spectrum remain "localized" in the mean-field basis. This is accompanied by a failure of ETH in that regime [31,32], and hence thermalization is *not expected* to occur when the energy of the time-evolving state after the quench is close to the ground-state energy (low effective temperatures). This is an important feature of isolated quantum systems that will need to be considered with more care when dealing with ultracold gases experiments. Second, in comparing bosons and fermions, larger fluctuations are verified for the latter,

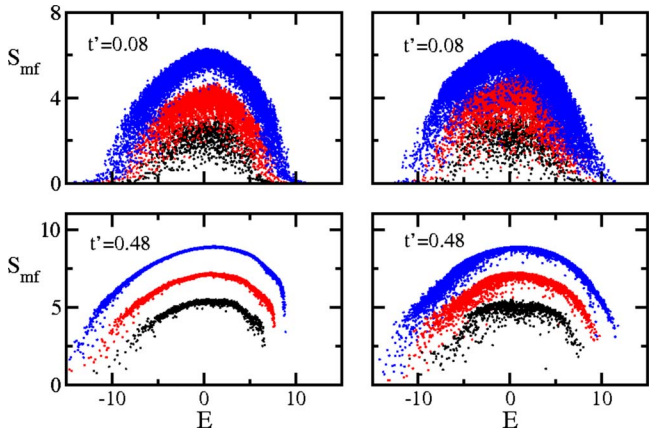

FIG. 8. (Color online) Shannon entropy in the mean-field basis vs energy when the system is close to integrability (top panels) and in the chaotic limit (bottom panels); $k=2$ and $t'=V'$. Panels on the left, bosons; panels on the right, fermions. Curves from bottom to top: $L=18,21,24$.

offering a further justification for the deviations between statistical-mechanics predictions for observables after relaxation and the exact time-averaged result of the quantum evolution observed in finite fermionic systems [32]. Note, however, that fluctuations appear to decrease with system size, as shown in Fig. 8 (especially noticeable in the bottom right panel). This may be a simple reflection of better statistics, but may suggest also that in the thermodynamic limit some of the differences between fermions and bosons may eventually disappear.

IV. CONCLUSIONS

We have presented a detailed analysis of the transition from integrability to quantum chaos for gapless one-dimensional systems of interacting spinless fermions and hard-core bosons. Here, the onset of chaos was dictated by the enhancement of next-nearest-neighbor hopping and interactions.

Our comparisons for different system sizes suggested that in the thermodynamic limit an infinitesimal integrability breaking term suffices for the onset of chaos, although further studies are necessary for settling this issue. Also, this may not warrant that thermalization will occur for infinitesimal integrability breaking terms since, at least for our finite systems, we could not establish a one-to-one correspondence between the two effects.

We have found differences in behaviors associated with particle statistics. The transition to chaos in fermionic systems, as measured by level spacing indicator, peak position of level spacing distribution, and level number variance, required integrability breaking terms larger than in the bosonic case. With respect to delocalization measures, larger fluctuations were also verified for fermions.

We studied wave-function complexity using different delocalization measures and choices of underlying basis. Our results have shown that the similar structure of eigenstates close in energy is a primary feature of chaotic systems. This finding reinforces the proposal to elevate Berry's conjecture to the status of the best definition of quantum chaos [20] and suggests that the onset of a smooth dependence of delocalization measures with energy be used as an indicator of quantum chaos and a condition for quantum thermalization.

Finally, we have shown that even when the systems are chaotic in terms of the level spacing distribution and the level number variance, there are still regions in the edges of the spectrum in which the states are less delocalized and their structures are less similar. As shown in Refs. [31,32], those states do not satisfy ETH and, hence, whenever one performs a quench in a system, so that the energy of the time-evolving state is close to the ground-state energy [or in other words, when the effective temperature of the system as defined by Eq. (7) is very low], relaxation of observables to the thermal distribution prediction is not expected.

The analysis and findings described here are intimately reflected by the studies of thermalization pursued in Refs. [25,31,32] and provide strong support to those works. Moreover, the lattices we considered may also be mapped onto other one-dimensional systems, such as spin-1/2 chains, which indicates the broad range of applicability of our results for gapless systems.

ACKNOWLEDGMENTS

L.F.S. thanks support from the Research Corporation. M.R. was supported by the U.S. Office of Naval Research and by Georgetown University.

APPENDIX: COMPLEXITY OF THE WAVE FUNCTIONS

We provide here further illustrations for the complexity increase of the wave functions with the onset of chaos for models (1) and (2). This is based on the computation of Shannon entropy [Eq. (5)] and the inverse participation ratio [Eq. (6)]. We compare results in both representations, mean-field and k-space bases. Overall, the approach to chaos is followed by the reduction in fluctuations in the results for S and IPR close in energy, with the decrease in fluctuations being slower for fermions than for bosons.

1. Effective temperature

Figures 6 and 7 gave the entropy in the mean-field basis vs the effective temperature. There, each temperature T_j, for an eigenstate of energy E_j, was obtained by means of Eq. (7) and performing the trace over the full spectrum (let us call it T_{all} here). In Fig. 9, we compare T_{all} with the eigenstate energies.

One may also wonder what would happen if one uses only the spectrum of the $k=2$ sector to perform the trace and hence to compute the temperature $T_{k=2}$. Actually, for the system sizes employed here, the values obtained in this latter way do not differ much from temperatures calculated considering the energies of all k sectors [60]. Figure 10 shows that the largest disagreements between T_{all} and $T_{k=2}$ occur at low energies; but even then, they are usually not higher than 5%. Exceptions are the first two or three lowest temperatures,

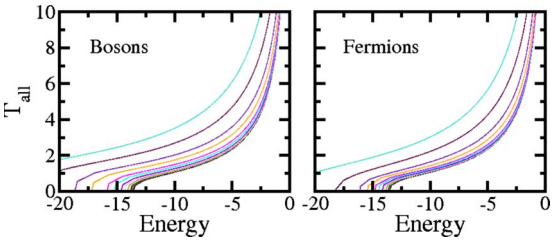

FIG. 9. (Color online) T_{all} vs energy, where T_{all} stands for the effective temperature computed considering the eigenvalues of all symmetry sectors; $L=24$. Curves from bottom to top: $t'=V'=0.00$, 0.02, 0.03, 0.04, 0.06, 0.08, 0.12, 0.16, 0.24, 0.32, 0.48, 0.64, 0.96, 1.28.

which do not appear in the scale of Fig. 10 due to significant discrepancies between T_{all} and $T_{k=2}$.

More generally, for larger system sizes, the temperature is expected to be computed by means of quantum Monte Carlo simulations or other better scaling numerical approaches. This means that in general all sectors will be considered when computing T. Our results here show that the differences with considering specific momentum sectors are small and decreasing with the system size.

2. Results in the mean-field basis

Figures 11 and 12 show the mean-field Shannon entropy vs energy for all the eigenstates of the $k=2$ sector. Notice

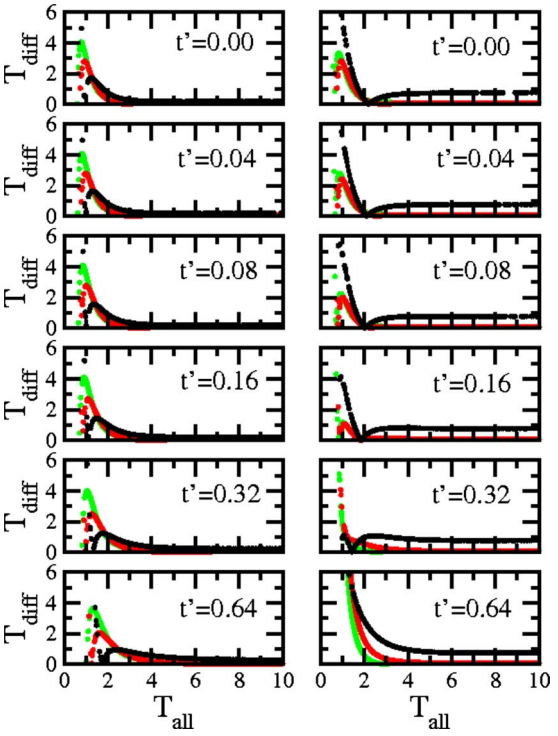

FIG. 10. (Color online) Temperature difference vs T_{all}. $T_{diff}=100|T_{all}-T_{k=2}|/T_{all}$, where $T_{k=2}$ is computed considering only the eigenvalues from the $k=2$ sector. Left panels, bosons; right panels, fermions; $t'=V'$. Negligible differences are seen between the curves for $L=24$ [light gray (green online)] and $L=21$ [dark gray (red online)] when $T_{all}>2$, while the curve for $L=18$ (black) saturates at a higher level (especially noticeable for fermions).

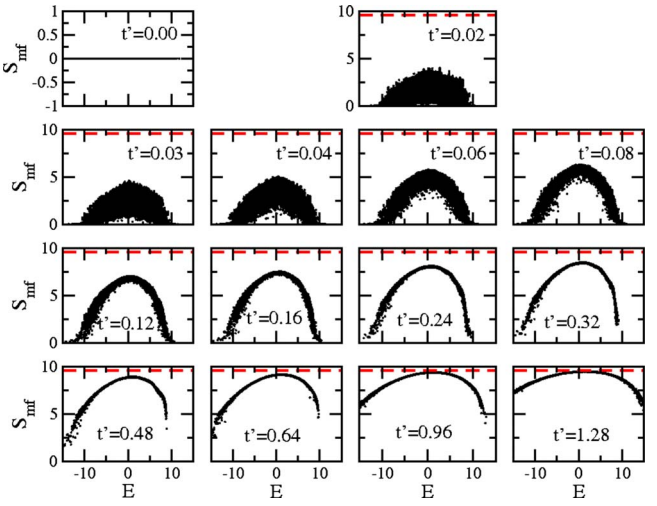

FIG. 11. (Color online) Shannon entropy in the mean-field basis vs energy for bosons; $L=24$, $k=2$, and $t'=V'$. The dashed line gives the GOE averaged value $S_{\mathrm{GOE}}\sim\ln(0.48D)$.

that the whole spectrum for the $k=2$ sector is presented and not only the energies leading to $T\leq 10$ as in Figs. 6 and 7. The typical behavior of banded matrices is observed: larger delocalization appearing away from the edges of the spectrum, although not as large as the GOE result $S_{\mathrm{GOE}}=\ln(0.48D)+\mathcal{O}(1/D)$, and lower complexity at the edges [13,15,57].

A similar behavior is seen in the plots of the inverse participation ratio in the mean-field basis vs energy (Figs. 13 and 14). The IPR values increase significantly with t',V', but do not reach the GOE result $\mathrm{IPR}=(D+2)/3$ [11,12]. IPR gives essentially the same information as S, although the first shows larger fluctuations.

3. Results in the k basis

Identifying the mean-field basis may not always be a simple task. For example, some 1D models may have more than one integrable point. It may also happen that one is so

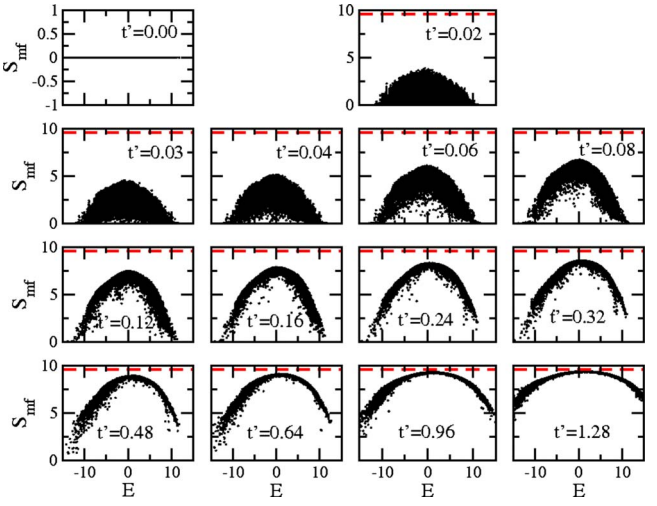

FIG. 12. (Color online) Same as in Fig. 11 for fermions.

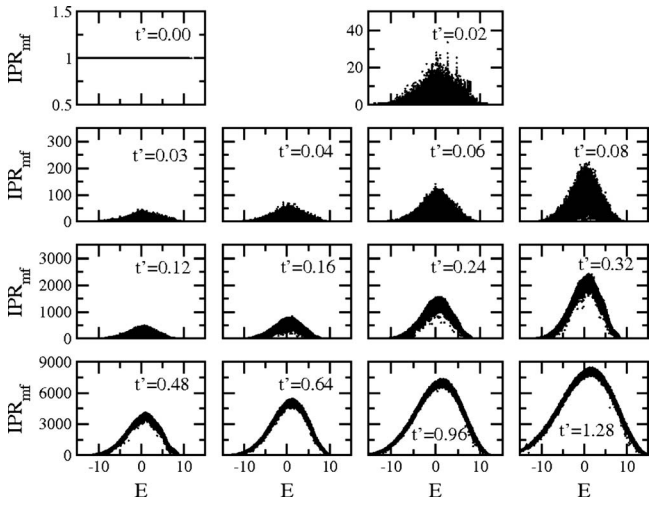

FIG. 13. Inverse participation ratio in the mean-field basis vs energy for bosons; $L=24$, $k=2$, and $t'=V'$. The GOE result $\mathrm{IPR}_{\mathrm{GOE}}\sim D/3$ is beyond the chosen scale.

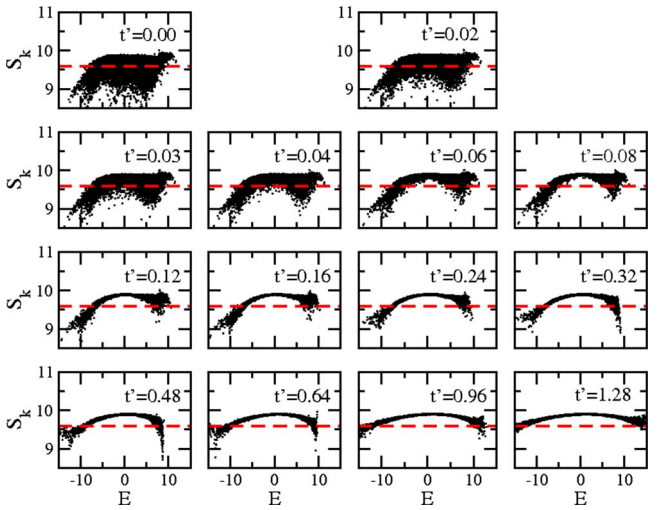

FIG. 15. (Color online) Shannon entropy in the k basis vs energy for bosons; $L=24$, $k=2$, and $t'=V'$. The dashed line gives the GOE averaged value $S_{\mathrm{GOE}}\sim\ln(0.48D)$.

far from any integrable point that there is no reason to believe that such a point has any relevance for the chosen system. The latter case may be particularly applicable to higher-dimensional systems where integrable points are, in general, the noninteracting limit or other trivial limit. Working on the mean-field basis also adds an extra step in the computations since the diagonalization of the system is usually not performed in that basis, i.e., one needs to perform a change in basis when computing S and IPR in the mean-field basis. This extra computation step may become very demanding when dealing with large systems. In addition, depending on the studies being performed, it may be of interest to analyze the structure of the eigenvectors in another basis. The problem of spatial localization, for example, calls for the use of the site basis.

Motivated by the discussion above, we include here the results for S in the k basis in which we diagonalize our Hamiltonians. Those are shown in Figs. 15 and 16. Large entropy values are now simply related to high delocalization with respect to the k basis and have nothing to do with the onset of chaos. They are found in both integrable and nonintegrable regimes and may even surpass S_{GOE}. Other differences between the mean-field and k bases include: (i) the localization increase expected for both edges of the spectrum in banded matrices is not so evident in the k basis, some high-energy states remaining as delocalized as the central states; and (ii) the distinct degree of fluctuations between bosons and fermions, even though still higher for fermions, is not so visible anymore. In spite of these deviations, the k basis may still be used as a signature of the integrable-chaos transition. The reason being that, just as in the mean-field basis, the dependence of S_k with energy becomes smoother *only* in the chaotic limit. Therefore, since reduction in fluctuations in S and IPR for states close in energy has been pointed as a main cause for the validity of the ETH, the k basis may still be used to determine where the onset of thermalization is expected.

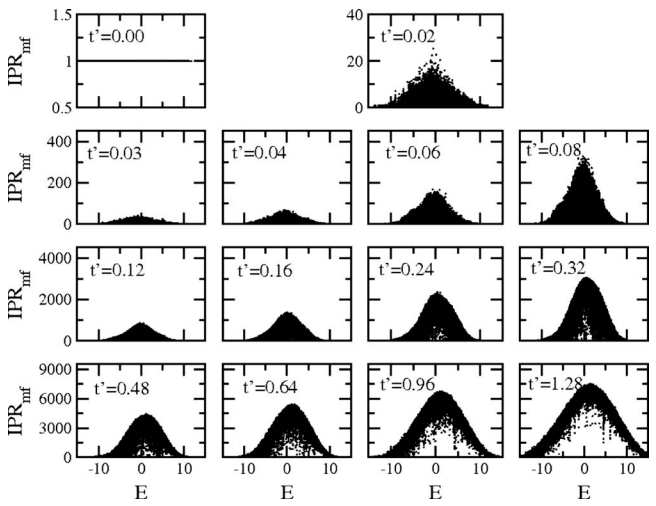

FIG. 14. Same as in Fig. 13 for fermions.

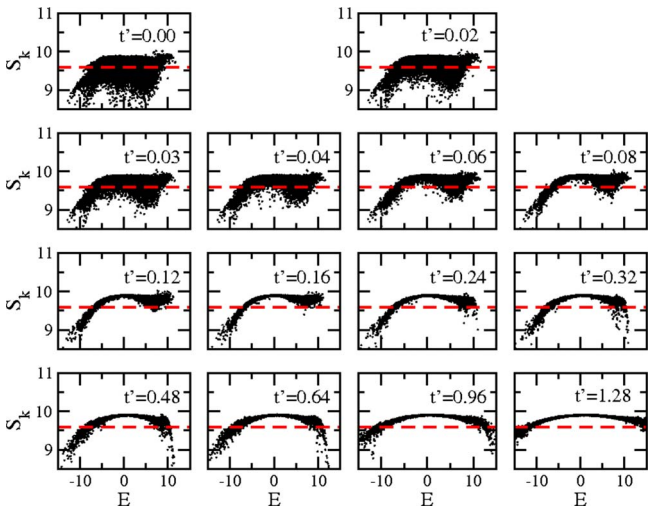

FIG. 16. (Color online) Same as in Fig. 15 for fermions.

[1] E. P. Wigner, Ann. Math. **53**, 36 (1951).
[2] M. L. Mehta, *Random Matrices* (Academic, Boston, 1991).
[3] G. Casati, F. Valz-Gris, and I. Guarneri, Lett. Nuovo Cimento Soc. Ital. Fis. **28**, 279 (1980).
[4] M. V. Berry, Ann. Phys. (N.Y.) **131**, 163 (1981).
[5] G. M. Zaslavsky, Phys. Rep. **80**, 157 (1981).
[6] O. Bohigas and M. Giannoni, *Lecture Notes in Physics* (Springer, Berlin, 1984), Vol. 209.
[7] F. Haake, *Quantum Signatures of Chaos* (Springer-Verlag, Berlin, 1991).
[8] T. Guhr, A. Mueller-Gröeling, and H. A. Weidenmüller, Phys. Rep. **299**, 189 (1998).
[9] Y. Alhassid, Rev. Mod. Phys. **72**, 895 (2000).
[10] L. E. Reichl, *The Transition to Chaos: Conservative Classical Systems and Quantum Manifestations* (Springer, New York, 2004).
[11] F. M. Izrailev, Phys. Rep. **196**, 299 (1990).
[12] V. Zelevinsky, B. A. Brown, N. Frazier, and M. Horoi, Phys. Rep. **276**, 85 (1996).
[13] V. K. B. Kota, Phys. Rep. **347**, 223 (2001).
[14] J. B. French and S. S. M. Wong, Phys. Lett. B **33**, 449 (1970).
[15] T. A. Brody, J. Flores, J. B. French, P. A. Mello, A. Pandey, and S. S. M. Wong, Rev. Mod. Phys. **53**, 385 (1981).
[16] J. Flores, M. Horoi, M. Müller, and T. H. Seligman, Phys. Rev. E **63**, 026204 (2001).
[17] D. J. Thouless, Phys. Rev. Lett. **39**, 1167 (1977).
[18] C. W. J. Beenakker, Rev. Mod. Phys. **69**, 731 (1997).
[19] J. M. Deutsch, Phys. Rev. A **43**, 2046 (1991).
[20] M. Srednicki, Phys. Rev. E **50**, 888 (1994).
[21] V. V. Flambaum, F. M. Izrailev, and G. Casati, Phys. Rev. E **54**, 2136 (1996).
[22] P. Jacquod and D. L. Shepelyansky, Phys. Rev. Lett. **79**, 1837 (1997).
[23] V. V. Flambaum and F. M. Izrailev, Phys. Rev. E **56**, 5144 (1997).
[24] F. M. Izrailev, in *New Directions in Quantum Chaos*, edited by G. Casati, I. Guarneri, and U. Smilansky, Proceedings of the International School of Physics Enrico Fermi No. 143 (IOS, Amsterdam, 2000), pp. 371–430.
[25] M. Rigol, V. Dunjko, and M. Olshanii, Nature (London) **452**, 854 (2008).
[26] M. Horoi, V. Zelevinsky, and B. A. Brown, Phys. Rev. Lett. **74**, 5194 (1995).
[27] T. Kinoshita, T. Wenger, and D. S. Weiss, Nature (London) **440**, 900 (2006).
[28] S. Hofferberth, I. Lesanovsky, B. Fischer, T. Schumm, and J. Schmiedmayer, Nature (London) **449**, 324 (2007).
[29] C. Kollath, A. M. Läuchli, and E. Altman, Phys. Rev. Lett. **98**, 180601 (2007).
[30] S. R. Manmana, S. Wessel, R. M. Noack, and A. Muramatsu, Phys. Rev. Lett. **98**, 210405 (2007).
[31] M. Rigol, Phys. Rev. Lett. **103**, 100403 (2009).
[32] M. Rigol, Phys. Rev. A **80**, 053607 (2009).
[33] I. E. Mazets, T. Schumm, and J. Schmiedmayer, Phys. Rev. Lett. **100**, 210403 (2008).
[34] A. Flesch, M. Cramer, I. P. McCulloch, U. Schollwöck, and J. Eisert, Phys. Rev. A **78**, 033608 (2008).
[35] G. Roux, Phys. Rev. A **79**, 021608(R) (2009).
[36] M. Rigol, e-print arXiv:0909.4556.
[37] G. Roux, e-print arXiv:0909.4620.
[38] Y. Avishai, J. Richert, and R. Berkovits, Phys. Rev. B **66**, 052416 (2002).
[39] L. F. Santos, J. Phys. A **37**, 4723 (2004).
[40] K. Kudo and T. Deguchi, Phys. Rev. B **69**, 132404 (2004).
[41] W. G. Brown, L. F. Santos, D. J. Starling, and L. Viola, Phys. Rev. E **77**, 021106 (2008).
[42] F. Dukesz, M. Zilbergerts, and L. F. Santos, New J. Phys. **11**, 043026 (2009).
[43] T. C. Hsu and J. C. Angles d'Auriac, Phys. Rev. B **47**, 14291 (1993).
[44] D. Poilblanc, T. Ziman, J. Bellissard, F. Mila, and G. Montambaux, EPL **22**, 537 (1993).
[45] D. A. Rabson, B. N. Narozhny, and A. J. Millis, Phys. Rev. B **69**, 054403 (2004).
[46] K. Kudo and T. Deguchi, J. Phys. Soc. Jpn. **74**, 1992 (2005).
[47] P. Jordan and E. Wigner, Z. Phys. **47**, 631 (1928).
[48] H. Bethe, Z. Phys. **71**, 205 (1931).
[49] M. Karbach and G. Müller, Comput. Phys. **11**, 36 (1997).
[50] J. M. G. Gómez, R. A. Molina, A. Relaño, and J. Retamosa, Phys. Rev. E **66**, 036209 (2002).
[51] L. F. Santos, J. Math. Phys. **50**, 095211 (2009).
[52] A. K. Zhuravlev, M. I. Katsnelson, and A. V. Trefilov, Phys. Rev. B **56**, 12939 (1997).
[53] L. F. Santos, D. Kusnezov, and Ph. Jacquod, Phys. Lett. B **537**, 62 (2002).
[54] M. Moeckel and S. Kehrein, Phys. Rev. Lett. **100**, 175702 (2008).
[55] M. Moeckel and S. Kehrein, Ann. Phys. (N.Y.) **324**, 2146 (2009).
[56] M. Eckstein, M. Kollar, and P. Werner, Phys. Rev. Lett. **103**, 056403 (2009).
[57] L. Kaplan and T. Papenbrock, Phys. Rev. Lett. **84**, 4553 (2000).
[58] I. Percival, J. Phys. B **6**, L229 (1973).
[59] M. V. Berry, J. Phys. A **10**, 2083 (1977).
[60] More generally, Ref. [12] has shown that different definitions of temperatures, associated with the microcanonical ensemble, single-particle occupation numbers, and information entropy, coincide in the chaotic regime.